Supporting Information for

Heterogeneous nucleation drives particle size segregation in sequential ozone and nitrate oxidation of catechol

Lauren A. Garofalo[1], Yicong He[2], Shantanu H. Jathar[2], Jeffrey R. Pierce[3], Carley D. Fredrickson[4], Brett B. Palm[4], Joel A. Thornton[4], Fabian Mahrt[5,6], Giuseppe V. Crescenzo[5], Allan K. Bertram[5], Danielle C. Draper[7,8], Juliane L. Fry[7], John Orlando[9], Xuan Zhang[9,10], Delphine K. Farmer[1*]*

* Corresponding authors: Lauren A. Garofalo, Lauren.Garofalo@colostate.edu

Delphine K. Farmer, Delphine.Farmer@colostate.edu

This document contains 13 pages.

S1. Experiment descriptions

The National Center for Atmospheric Research (NCAR) Atmospheric Simulation Chamber in Boulder, CO is a 10 m^3 FEP Teflon (0.005") bag in a cubic enclosure with UV-reflective surfaces. The chamber features a bank of 128 wall-mounted blacklight tubes (32W, Type F32T8/BL) that were set to 100% (J_{NO2} = 1.24 x 10^{-3} s^{-1}) for all photooxidation experiments. During the experiments described herein, the chamber temperature ranged from 22-35 °C, increasing during experiments with UV lights due to heat generation. Each experiment was conducted under dry conditions (RH <10%). The chamber was flushed with particle and VOC-free air overnight between experiments. The chamber was passively mixed without fans. In the experiments described here, we filled the chamber with zero air, injected reagents in discrete events, and sampled the reagents and products in the chamber continuously. For some experiments, the UV lights were turned on at the end of the SOA formation experiment to monitor changes in the SOA composition and optical properties over several hours.

Catechol + OH/NO_x [190603]

Injected H_2O_2. Two hours later, HONO from reaction of 3 mL 10% wt sulfuric acid and 3 mL 1% wt sodium nitrate was added. After 30 min to allow mixing, 60 ppb catechol was injected, followed by dry $(NH_4)_2SO_4$ particles (ammonium sulfate; AS). An additional 10 ppb of catechol was injected. After 1 hr to allow for the reagents to mix, the UV lights were turned on and the experiment ran for 6 hours. Immediately before turning the lights on, NO = 149 ppb, NO_2 = 99 ppb, AS = 100 µg m^{-3}, catechol = 40 ppb, and HONO = 20 ppb.

Catechol + NO_3 [190604]

Injected 140 ppb O_3. After 30 min to allow mixing, 60 ppb catechol was injected. After an additional 30 min, 100 µg m^{-3} dry $(NH_4)_2SO_4$ seed was injected. It was observed that catechol and ozone reacted to form SOA, so an additional 10 ppb of catechol was injected. After 2 hours of mixing, 80 ppb NO_2 was injected. Immediately before the NO_2 was injected, O_3 = 195 ppb, NO_2 = 0.2 ppb, SOA = 5 µg m^{-3}, AS = 150 µg m^{-3}. An hour after the initial NO_2 was injected, additional O_3 and NO_2 was added. The experiment was completed 4 hours after the initial NO_2 injection, which was considered t= 0.

Catechol + NO_3 [190605]

Injected 170 ppb O_3 in incremental steps. Inject 70 ppb catechol. After 30 min, 100 µg m^{-3} AS seed was injected. After one hour, 90 ppb NO_2 was injected, marking the beginning of the experiment. Immediately before the NO_2 injection, O_3 = 177 ppb, catechol = 40 ppb, AS seed = 170 µg m^{-3}, SOA = 5 µg m -3.

Forty minutes after the initial NO_2 addition, O_3 and NO_2 were added. To investigate the effect of photochemistry on the products of the dark chemistry, the UV lights were turned on and the products were monitored overnight. The initial NO_2 addition was considered t=0.

Catechol + NO_3 [190614]

This experiment replicated the 190605 experiment. Inject 130 ppb O_3. 50 min later, inject catechol. After 30 min, inject $(NH_4)_2SO_4$ seed. After 40 additional minutes, NO_2 and O_3 were added to the chamber. Immediately before the NO_2 injection, O_3 = 115 ppb, catechol = 52 ppb, AS = 150 μg m^{-3}. Approximately 3 hours after the initial NO_2 injection, NO was added to titrate the remaining O_3. Then the UV lights were turned on to monitor the further photooxidation of the SOA products overnight. 2ppm of butanol was injected at the end of the experiment. The initial NO_2 addition was considered t=0.

Instrument descriptions

Size-resolved chemically speciated aerosol mass concentrations were measured by high-resolution time-of-flight aerosol mass spectrometry (HR-AMS; Aerodyne, Inc) [1]. This instrument was operated with "V" ion-path (m/Δm = 2500) in both mass spectra (MS) and particle time-of-flight (PTOF) modes, typically with timing of 5 s open, 5 s closed, and 10 s PTOF for 3, 15, or 30 cycles resulting in 1, 5, 10 min sample intervals. The AMS was operated with lens pressure of 1.5 Torr, using a 120 μm critical orifice at an elevation of ~1500m asl. The raw data was processed in the High Resolution TOF-AMS Analysis Toolkit v1.20 (Aerodyne, Inc.) in Igor Pro 7 (Wavemetrics, Inc.). Filter periods during the experiments were used to determine the CO_2 correction to accurately remove the contribution of gas phase CO_2 to the CO_2^+ ion signal and determine detection limits. We calibrated the instrument intake for standard flow, size-dependent particle velocity with PSL standards (60-750 nm), ionization efficiency (IE) with size-selected NH_4NO_3, and relative IE with size-selected $(NH_4)_2SO_4$. We report MOONLIGHT data with a collection efficiency of 0.65 based on previous field data [2].

Particle size distributions were also measured with a scanning particle mobility sizer (SMPS; TSI, Inc.) consisting of a differential mobility analyzer (DMA; TSI 3080) and condensation particle counter (CPC; TSI 7610). The SMPS counted particles in 20 bins between mobility diameters 24 nm and 457 nm.

Gas phase measurements included O_3, NO and NO_2, and volatile organic compounds. O_3 was measured with a UV-absorption ozone monitor (Model 49i-PIS, ThermoScientific) and NO_x ($NO + NO_2$) with a chemiluminescence NO detector (Model CLD 88Y, EcoPhysics) coupled to a catalyst to convert NO_2 to NO.

Gas phase mixing ratios of phenolic compounds, H_2O_2, and HNO_2 were measured using chemical ionization mass spectrometry using iodide reagent ion (I-CIMS) [3]. The I-CIMS was operated with a Filter Inlet for Gases and AEROsols (FIGAERO)[4] to measure both gas and particle phases. During the particle collection/gas sampling mode, the FIGAERO collects particles on a filter for a ten-minute period while sampling the gas phase with ion-molecule reaction (IMR) region flushing with N_2 (zeroing) every two minutes. During particle sampling mode, the filter is heated with steadily increasing temperatures from room temperature to ~200 ^oC at 10 ^oC per minute and then held at ~ 200 ^oC for the remainder of an hour to quantify volatilized compounds. Time-integrated and blank corrected signal, where the filter blank is obtained by heating the filter with no particle collection) is reported as particle mass concentration every seventy minutes. Nitrocatechol was calibrated by injecting a diluted solution of nitrocatechol, acetone, and methanol onto a filter already positioned within the sampling tube while actively sampling into the CIMS. With this setup, all evaporative losses would be drawn into the CIMS to be measured and the total nitrocatechol mass would be measured by the CIMS."

In the catechol + O_3 + NO_3 experiments, FIGAERO I-CIMS particulate nitrocatechol exceeded the AMS bulk OA, but this was not the case in the catechol + OH/NO_x experiment. Additionally, the FIGAERO I-CIMS nitrocatechol decreased after initial production, while the HR-AMS bulk OA slightly increased before decreasing at a slower rate than that measured by the FIGAERO I-CIMS. Also, in the larger OA particle size mode, as reported with the HR-AMS in catechol + O_3 + NO_3 experiments, the size distribution decreased near the HR-AMS size cutoff. With these observations, we suspect the differences in the HR-AMS and FIGAERO I-CIMS are due to differences in particle size cuts whereby the AMS does not detect particle mass contained in particles larger than 1 um, most of which is nitrocatechol. Particle wall-loss of OA may be offset by continued ozonolysis of secondary products to form additional OA mass. This is consistent with the observation that OA increases in the AMS measurements, but the FIGAERO-CIMS data shows a decrease in nitrocatechol. Nevertheless, the development and characterization of the segregated aerosol population at larger sizes, of almost exclusively nitrocatechol, is unaffected by differences in the particle size cuts for the FIGAERO-CIMS and HR-AMS.

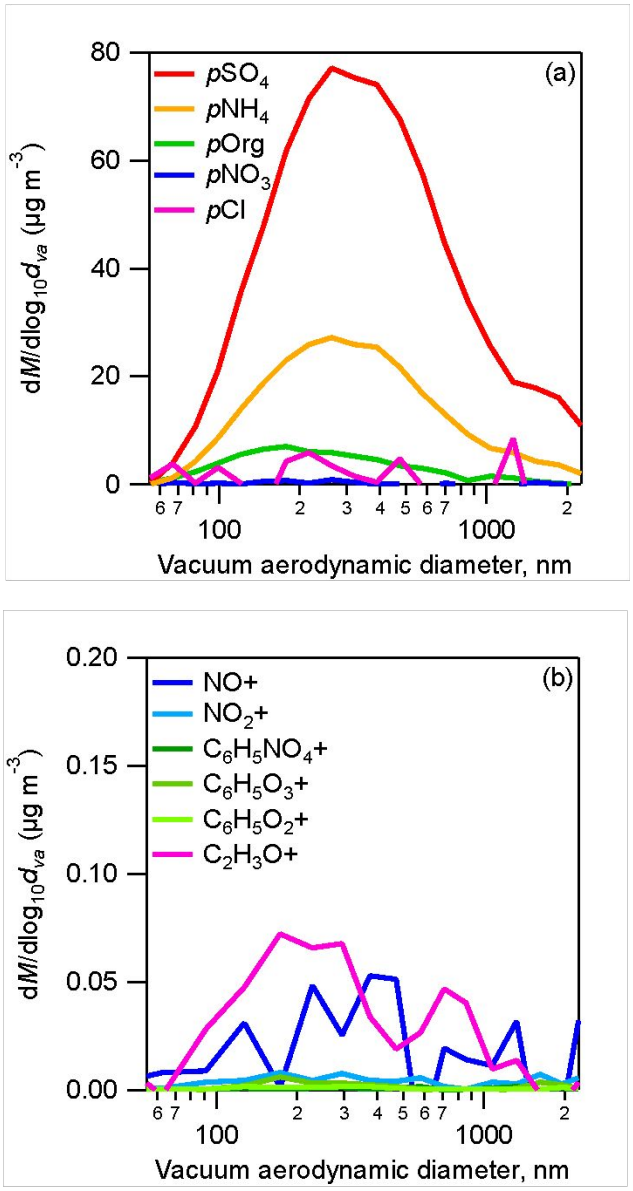

Figure S1. Size-distribution for catechol + O_3 + NO_3 oxidation before NO_2 was injected into the chamber for (a) bulk chemical species and (b) selected high-resolution ions: pNO_3 components (NO^+, NO_2^+); the nitrocatechol molecular ion and fragment ions ($C_6H_5NO_4^+$, $C_6H_5O_3^+$, $C_6H_5O_2^+$); and a smaller oxidized organic fragment ($C_2H_3O^+$). The organic aerosol signal is from SOA formed from the ozonolysis of catechol and the particle size distributions for the high resolution ions are noisier due to lower signal, however we see that the existing organic aerosol mode has one mode and is shifted to slightly smaller sizes compared to the seed aerosol.

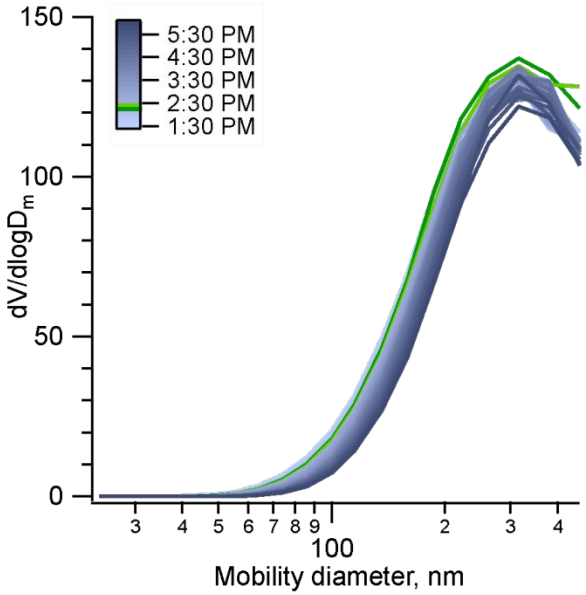

Figure S2. SMPS volume distributions for June 4 experiment (catechol + O_3 + NO_3 reaction). Time traces are colored from light to dark in 10 min intervals, with the time periods for which a larger size distribution is beginning to be observed in green. The green traces occur at the start of nitrocatechol production and growth of larger size mode at ~2:15 pm after NO_2 injection.

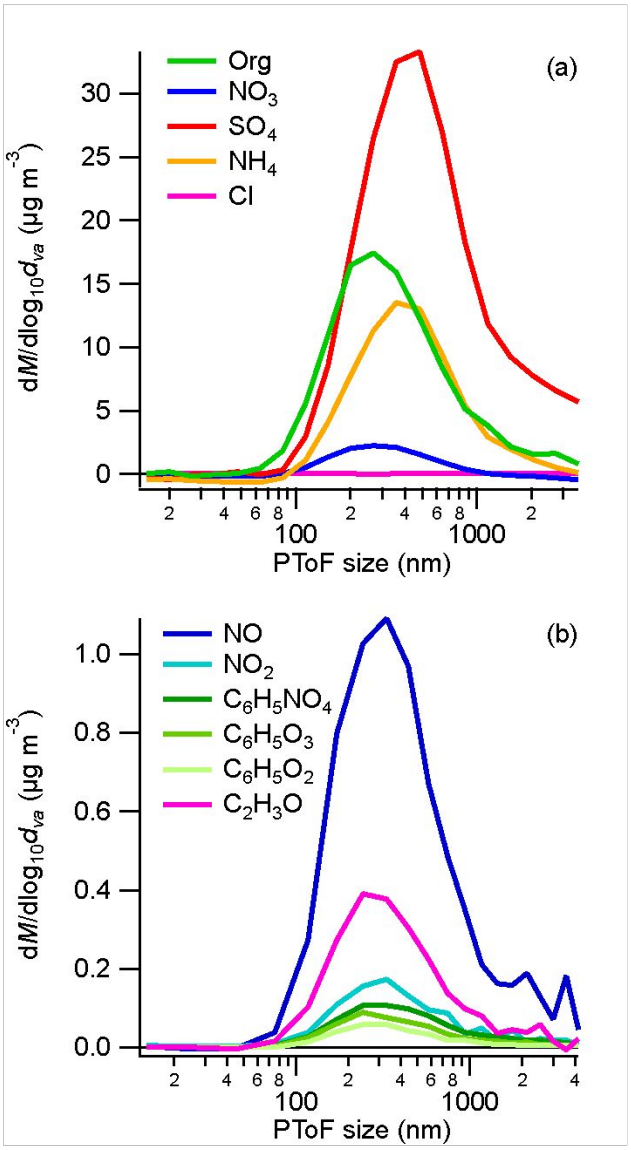

Figure S3. Size distributions for (a) bulk aerosol species and (b) high-resolution ions, as in Figure 2, for the catechol + OH/NO_x experiment at maximum OA concentrations.

S2. Additional model description

Table S1. Model Inputs and Features

Model species	NC-SOA: nitrocatechol SOA, C^*=13 and 3[#] μg m^{-3}, formation informed by HR-AMS measurements
	O_3-SOA: initial SOA, C^*=0.1 μg m^{-3}, initial state informed by SMPS and HR-AMS measurements (mass = 7.7 μg m^{-3}, mass median diameter = 280nm, geometric standard deviation = 2.1), D_b = 10^{-6} and 10^{-15}[#] cm^2 s^{-1}
	nonNC-SOA: non-nitrocatechol SOA, C^*=10^{-6} μg m^{-3}, formation informed by HR-AMS measurements
Heterogeneous nucleation	Surface tension (γ = 0.079 and 0.025[#] N m^{-1}), particle density (ρ=1400 kg m^{-3})
Environmental conditions	Temperature = 298 K
Wall losses	Sensitivity simulations performed with vapor and particle wall loss modeled based on measurements performed on the Colorado State University 10 m^3 chamber (k_e=0.13 s^{-1} and $k_{vap,on}$=1.28×10^{-3} s^{-1}; k_e=0.13 s^{-1} and $k_{w,p0}$=4.44 x 10^{-6} s^{-1}) [5, 6]

[#]inputs for sensitivity simulations

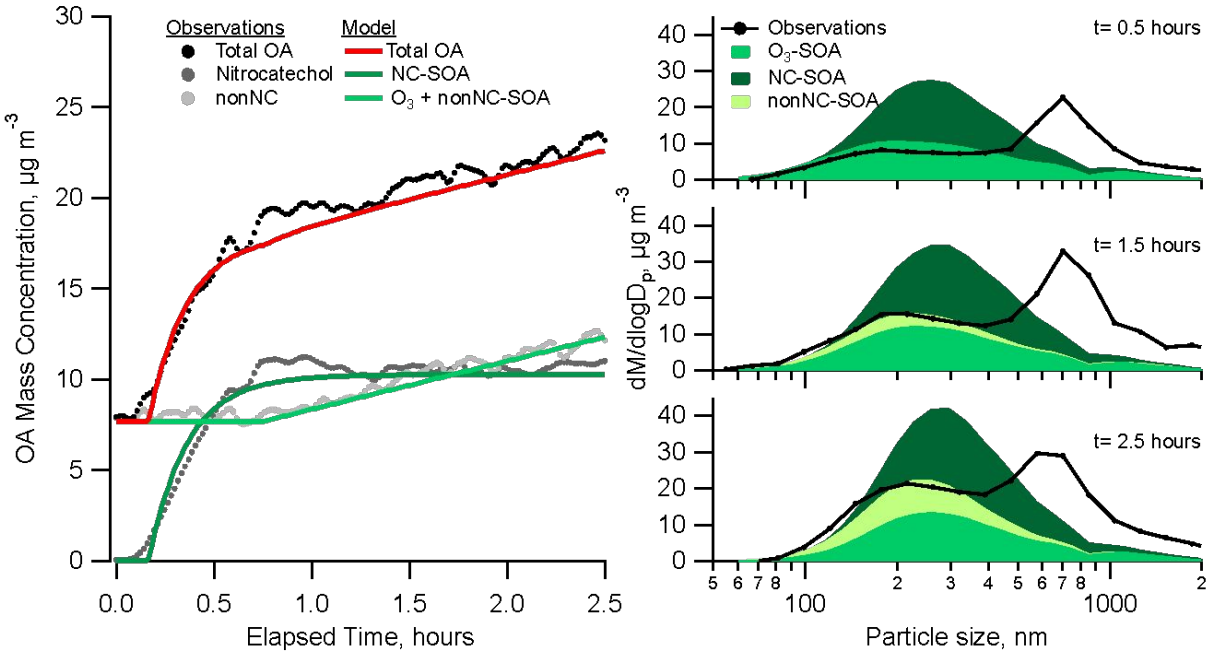

Figure S4. Model results, as in Figure 4, assuming condensation without the heterogeneous nucleation scheme. Nitrocatechol and other species condense to the surface area size distribution as expected for lower volatility species.

S.3 Viscosity measurement description

Secondary organic aerosol (SOA) from dark ozonolysis of catechol was produced in a continuous flow environmental chamber at the University of British Columbia. The chamber, which consists of a flexible Teflon bag (Ingeniven) with an aluminum enclosure, has a volume of 1.8 m^3, and has been described in detail elsewhere.[7] For SOA generation, a mixture (1.75 wt %) of catechol dissolved in 2-butanol was continuously injected into a heated (387 K) glass bulb. Upon vaporization the catechol was carried into the chamber by dry and hydrocarbon free air (1.5 L min^{-1}), produced by a zero-air generator (Aadco, model 737). Similarly, O_3 was continuously generated and fed into the chamber by passing dry and hydrocarbon free air (1.3 L min^{-1}) through an O_3 generator, consisting of a mercury discharge lamp (Jelight, model 610). Catechol at the chamber inlet were approximately 315 ± 15 ppb and for all experiments, the relative humidity (RH) was below 1.5%, the temperature was 298 ± 2 K, and the residence time in the chamber was approximately 1.6 h for the flow rates used. The mass loading of SOA particles at the exit of the environmental chamber was around 85µg m^{-3}, as determined with an optical particle counter (Grimm, model 11-S) and the O_3 concentration at the chamber exit was 200 ± 30 ppb, as monitored with an O_3 detector (Thermo Scientific, 49i). SOA particles were collected at the exit of the

environmental chamber onto 12 mm diameter glass slides (Hampton Research, HR3-277) that had been made hydrophobic by coating the slides with Trichloro(1H,1H,2H,2H-perfluorooctyl)silane. Aerosol particles were collected onto the hydrophobic glass slides using a single-stage impactor (MOSSI, MPS Corporation; 50% aerodynamic cut-diameter of 0.18 μm), operated for ~24 h at a flow rate of 13 L min^{-1}. During collection, sub-micrometer SOA particles coagulated on the hydrophobic glass slides to form super-micrometer SOA particles around 60 μm in diameter, with roughly a spherical cap geometry.

The viscosity of the collected SOA was subsequently determined using the poke-flow technique, which has been developed to measure the viscosity of small samples (~1 mg) having viscosities between 10^9 and 10^3 Pa s.[8, 9] To perform the poke-flow measurements, the slide with the collected SOA particles was placed into a RH-controlled flow cell, which is coupled to an inverted optical microscope (AmScope, model ME1400TC-INF). Before performing a poke-flow experiment, the SOA particles were conditioned directly within the flow for a period between 2 to 23 h at RH values less than 1.5%, by continuously passing a flow (~0.5 L min^{-1}) of nitrogen gas (5.0 grade, Praxair) over the particles. The viscosity results did not depend on the conditioning time (Figure S5). After conditioning the particles for 2 to 23 h, individual particles were poked with a sharp, oleophobic-coated (CYTONIX, OilSlip 110), ultrafine (20 μm tip diameter) tungsten needle (Roboz Surgicial Instruments Co.). The poking process typically results in the SOA particles forming roughly a half torus geometry with an inner diameter of ~25 μm. The morphological evolution of the poked particles was then monitored by taking optical microscope images with a digital camera (AmScope, MA1000). If the viscosity is not too high (less than 10^7 Pa s), the material flows and returns to the initial spherical cap geometry for typical experimental timescales, to minimize the surface energy of the system. In the current experiments, however, the SOA material was too viscous to flow significantly during our experimental timescales (2 to 4 h)

To determine the viscosity of the SOA, the behavior observed in the experiments were simulated using the COMSOL Multiphysics® (COMSOL Inc., v5.4) software package with the Microfluidics Module. The geometry used in the simulations was identical to the experiments. The viscosity in the simulations was systematically adjusted until the material in the simulations flowed by 0.5 μm, in the same amount of time as used in the experiments (2 to 4 h). A flow distance of 0.5 μm is the maximum amount of flow that could have occurred in our experiments based on the resolution of our optical microscope. Since a flow distance of 0.5 micrometers is an upper limit, the viscosities from the simulations denote lower limits. Input parameters of the COMSOL Multiphysics® fluid simulations include the surface tension, the slip length, the density of the SOA material, as well as its contact angle on the substrate. The values used in the simulations for catechol + O_3 SOA at RH values below 1.5% are given in Table S1. For the density,

we assumed a value of 1 g cm^{-3}, the simulated viscosity did not depend on this value. For the surface tension, we used the surface tension of liquid catechol, determined with the PhysChem Module of the ACD/Labs Percepta Platform. This should be a lower limit to the surface tension of the SOA, since surface tension should increase as oxidation increases. A lower limit to surface tension results in a lower limit to the simulated viscosity. For the contact angle, we used values determined experimentally with a confocal microscope following a previously described method.[10] For the slip length, we used a lower limit to the values reported in the literature.[11-23] A lower limit to the slip length results in a lower limit to the simulated viscosity.

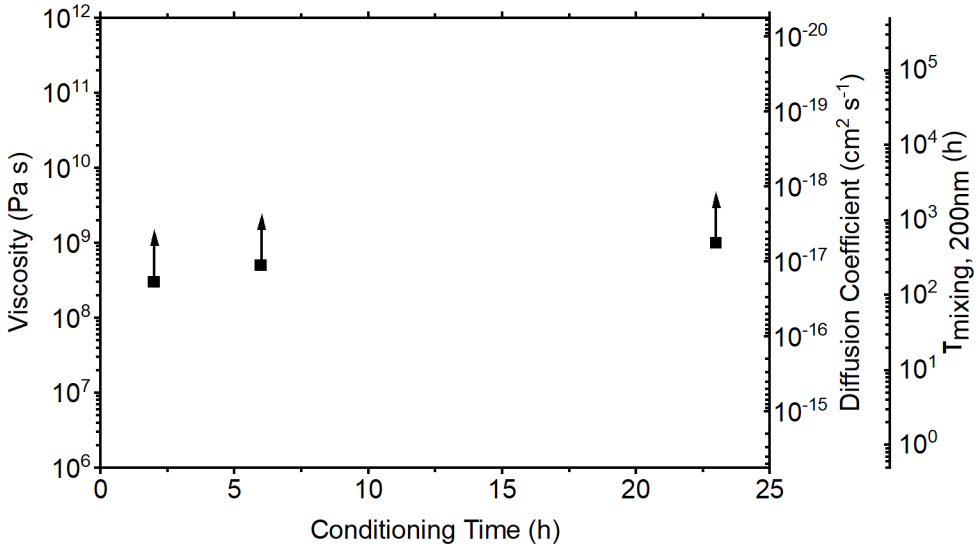

Figure S5: Lower limits of viscosities, diffusion coefficients, and mixing times determined for the catechol + O_3 SOA. The conditioning time corresponds to the time used to condition the particles to the surrounding RH (less than 1.5%) prior to poking the particles.

Shown in Figure S5 (left y-axis) are the lower limits of the viscosities determined for the catechol + O_3 SOA. Based on the results shown in Figure S5, we conclude that the viscosity of the catechol + O_3 SOA is greater than 3×10^8 Pa s, and independent of the time the particles were conditioned to the surrounding RH prior to poking the particles. Corresponding diffusion coefficients of organic molecules within the catechol + O_3 SOA were calculated from the determined viscosity values using the Stokes-Einstein equation, following previous methods.[24, 25]

$$D_{\mathrm{org}} = \frac{k_{\mathrm{B}}T}{6\pi\eta r}. \qquad \text{(S1)}$$

Here, k_B denotes the Boltzmann constant, T is temperature in Kelvin, η is the simulated viscosity in Pa s. Furthermore, r denotes the hydrodynamic radius of the diffusing organic molecules. Assuming r = 0.38 nm, the diffusion coefficient, D_{org}, is less than 2×10^{-17} cm^2 s^{-1} (see Figure S5 right hand y-axis). Finally, the mixing time of organic molecules within a 200 nm SOA particle. $T_{mixing,\ 200\ nm}$, was calculated using the following equation:[24,25]

$$\tau_{\text{mixing, 200 nm}} = \frac{d_p^2}{4\pi^2 D_{org}}, \qquad \text{(S2)}$$

where, d_p = 200 nm. The mixing time corresponds to the time for the concentration of diffusing organics at the center of the SOA particle to change by less than 1/e of the equilibrium concentration. Using a diffusion coefficient of 2×10^{-17} cm^2 s^{-1} corresponds to a $T_{mixing,\ 200\ nm}$ value of approximately 150 h.

Table S2: Input parameters used in the COMSOL Multiphysics® simulations of the poke-flow experiments, to estimate a lower limit of viscosity for the catechol + O_3 SOA particles at less than 1.5% RH and T = 298 K.

SOA	Surface tension (N m^{-1})	Slip length (m)	Contact angle (°)	Density (g cm^{-3})
Catechol+O_3 SOA	0.0575[a]	5×10^{-9}[b]	70.4 ± 23.2[c]	1.0[d]

[a]Surface tension of pure catechol. Surface tensions were determined with the ACD/Labs Percepta Platform-PhysChem Module, retrieved from Chemspider July 12, 2020. [b]Lower limit to the reported slip length values, based on measurements of the slip length of organic compounds and water on hydrophobic surfaces.[11-23] [c]Contact angle, as determined by measuring the height and radii of individual droplets using a confocal microscope following previous methods.[10] [d]We assumed a value of 1 g cm^{-3}, the simulated viscosity did not depend on this value.

References

1. DeCarlo, P. F.; Kimmel, J. R.; Trimborn, A.; Northway, M. J.; Jayne, J. T.; Aiken, A. C.; Gonin, M.; Fuhrer, K.; Horvath, T.; Docherty, K. S.; Worsnop, D. R.; Jimenez, J. L., Field-deployable, high-resolution, time-of-flight aerosol mass spectrometer. *Anal Chem* **2006,** *78* (24), 8281-8289.
2. Garofalo, L. A.; Pothier, M. A.; Levin, E. J. T.; Campos, T.; Kreidenweis, S. M.; Farmer, D. K., Emission and Evolution of Submicron Organic Aerosol in Smoke from Wildfires in the Western United States. *Acs Earth Space Chem* **2019,** *3* (7), 1237-1247.
3. Lopez-Hilfiker, F. D.; Iyer, S.; Mohr, C.; Lee, B. H.; D'Ambro, E. L.; Kurten, T.; Thornton, J. A., Constraining the sensitivity of iodide adduct chemical ionization mass spectrometry to multifunctional organic molecules using the collision limit and thermodynamic stability of iodide ion adducts. *Atmos Meas Tech* **2016,** *9* (4), 1505-1512.
4. Lopez-Hilfiker, F. D.; Mohr, C.; Ehn, M.; Rubach, F.; Kleist, E.; Wildt, J.; Mentel, T. F.; Lutz, A.; Hallquist, M.; Worsnop, D.; Thornton, J. A., A novel method for online analysis of gas and particle composition: description and evaluation of a Filter Inlet for Gases and AEROsols (FIGAERO). *Atmos Meas Tech* **2014,** *7* (4), 983-1001.
5. He, Y.; Akherati, A.; Nah, T.; Ng, N. L.; Garofalo, L. A.; Farmer, D. K.; Shiraiwa, M.; Zaveri, R. A.; Cappa, C. D.; Pierce, J. R.; Jathar, S. H., Particle Size Distribution Dynamics Can Help Constrain the Phase State of Secondary Organic Aerosol. *Environ Sci Technol* **2021**, 1466–1476.
6. Bian, Q. J.; Jathar, S. H.; Kodros, J. K.; Barsanti, K. C.; Hatch, L. E.; May, A. A.; Kreidenweis, S. M.; Pierce, J. R., Secondary organic aerosol formation in biomass-burning plumes: theoretical analysis of lab studies and ambient plumes. *Atmos Chem Phys* **2017,** *17* (8), 5459-5475.
7. Maclean, A. M.; Smith, N. R.; Li, Y.; Huang, Y.; Hettiyadura, A. P. S.; Crescenzo, G. V.; Shiraiwa, M.; Laskin, A.; Nizkorodov, S. A.; Bertram, A. K., Humidity-Dependent Viscosity of Secondary Organic Aerosol from Ozonolysis of β-Caryophyllene: Measurements, Predictions, and Implications. *Acs Earth Space Chem* **2021**.
8. Renbaum-Wolff, L.; Grayson, J. W.; Bateman, A. P.; Kuwata, M.; Sellier, M.; Murray, B. J.; Shilling, J. E.; Martin, S. T.; Bertram, A. K., Viscosity of α-pinene secondary organic material and implications for particle growth and reactivity. *Proceedings of the National Academy of Sciences* **2013,** *110* (20), 8014-8019.
9. Grayson, J.; Song, M.; Sellier, M.; Bertram, A., Validation of the poke-flow technique combined with simulations of fluid flow for determining viscosities in samples with small volumes and high viscosities. *Atmospheric Measurement Techniques Discussions* **2015,** *8* (1).
10. Chesna, J. W.; Wiedmaier, B. F.; Wang, J.; Samara, A.; Leach, R. K.; Her, T.-H.; Smith, S. T., Aerial wetting contact angle measurement using confocal microscopy. *Measurement Science and Technology* **2016,** *27* (12), 125202.
11. Churaev, N.; Sobolev, V.; Somov, A., Slippage of liquids over lyophobic solid surfaces. *Journal of Colloid and Interface Science* **1984,** *97* (2), 574-581.
12. Bhattarai, H.; Saikawa, E.; Wan, X.; Zhu, H. X.; Ram, K.; Gao, S. P.; Kang, S. C.; Zhang, Q. G.; Zhang, Y. L.; Wu, G. M.; Wang, X. P.; Kawamura, K.; Fu, P. Q.; Cong, Z. Y., Levoglucosan as a tracer of biomass burning: Recent progress and perspectives. *Atmos Res* **2019,** *220*, 20-33.

13. McBride, S. P.; Law, B. M., Viscosity-dependent liquid slip at molecularly smooth hydrophobic surfaces. *Physical Review E* **2009,** *80* (6), 060601.
14. Bhushan, B.; Wang, Y.; Maali, A., Boundary slip study on hydrophilic, hydrophobic, and superhydrophobic surfaces with dynamic atomic force microscopy. *Langmuir* **2009,** *25* (14), 8117-8121.
15. Cottin-Bizonne, C.; Cross, B.; Steinberger, A.; Charlaix, E., Boundary slip on smooth hydrophobic surfaces: Intrinsic effects and possible artifacts. *Physical review letters* **2005,** *94* (5), 056102.
16. Baudry, J.; Charlaix, E.; Tonck, A.; Mazuyer, D., Experimental evidence for a large slip effect at a nonwetting fluid− solid interface. *Langmuir* **2001,** *17* (17), 5232-5236.
17. Joseph, P.; Tabeling, P., Direct measurement of the apparent slip length. *Physical Review E* **2005,** *71* (3), 035303.
18. Cottin-Bizonne, C.; Jurine, S.; Baudry, J.; Crassous, J.; Restagno, F.; Charlaix, E., Nanorheology: An investigation of the boundary condition at hydrophobic and hydrophilic interfaces. *The European Physical Journal E* **2002,** *9* (1), 47-53.
19. Cho, J.-H. J.; Law, B. M.; Rieutord, F., Dipole-dependent slip of Newtonian liquids at smooth solid hydrophobic surfaces. *Physical review letters* **2004,** *92* (16), 166102.
20. Vinogradova, O. I.; Koynov, K.; Best, A.; Feuillebois, F., Direct measurements of hydrophobic slippage using double-focus fluorescence cross-correlation. *Physical review letters* **2009,** *102* (11), 118302.
21. Jing, D.; Bhushan, B., Boundary slip of superoleophilic, oleophobic, and superoleophobic surfaces immersed in deionized water, hexadecane, and ethylene glycol. *Langmuir* **2013,** *29* (47), 14691-14700.
22. Tretheway, D. C.; Meinhart, C. D., Apparent fluid slip at hydrophobic microchannel walls. *Physics of fluids* **2002,** *14* (3), L9-L12.
23. Craig, V. S.; Neto, C.; Williams, D. R., Shear-dependent boundary slip in an aqueous Newtonian liquid. *Physical review letters* **2001,** *87* (5), 054504.
24. Seinfeld, J. H.; Pandis, S. N., *Atmospheric Chemistry and Physics: From Air Pollution to Climate Change*. John Wiley: Hoboken, N.J., 2006.
25. Shiraiwa, M.; Ammann, M.; Koop, T.; Pöschl, U., Gas uptake and chemical aging of semisolid organic aerosol particles. *Proceedings of the National Academy of Sciences* **2011,** *108* (27), 11003-11008.